



Published in final edited form as:

*Integr Biol (Camb)*. 2015 December ; 7(12): 1526–1533. doi:10.1039/c5ib00208g.

## Collective Motion of Mammalian Cell Cohorts in 3D

Yasha Sharma<sup>a</sup>, Diego A. Vargas<sup>a</sup>, Adrian F. Pegoraro<sup>b</sup>, David Lepzelter<sup>a</sup>, David A. Weitz<sup>b</sup>, and Muhammad H Zaman<sup>a,\*</sup>

<sup>a</sup>Department of Biomedical Engineering, Boston University, Boston, Massachusetts 02215

<sup>b</sup>School of Engineering and Applied Sciences, Harvard University, Cambridge, Massachusetts 02138

### Abstract

Collective cell migration is ubiquitous in biology, from development to cancer; it occurs in complex systems comprised of heterogeneous cell types, signals and matrices, and requires large scale regulation in space and time. Understanding how cells achieve organized collective motility is crucial to addressing cellular and tissue function and disease progression. While current two-dimensional model systems recapitulate the dynamic properties of collective cell migration, quantitative three-dimensional equivalent model systems have proved elusive. To establish such a model system, we study cell collectives by tracking individuals within cell cohorts embedded in three dimensional collagen scaffolding. We develop a custom algorithm to quantify the temporal and spatial heterogeneity of motion in cell cohorts during motility events. In the absence of external driving agents, we show that these cohorts rotate in short bursts, <2 hours, and translate for up to 6 hours. We observe, track, and analyze three dimensional motion of cell cohorts composed of 3–31 cells, and pave a path toward understanding cell collectives in 3D as a complex emergent system.

### Keywords

cell migration; collective motion; collagen matrices; cell-cell interactions; E-cadherin; collective cell migration; emergent systems; 3D; 3D culture

### Introduction

From early development to morphogenesis, wound healing, and even in cancer pathologies, biological function hinges on collective cell migration. Currently, studies of the inter-cellular dynamics of collective cell motion are primarily conducted via two dimensional (2D) monolayer experiments. Here we present a 3-dimensional study of cell collectives.

Cells must coordinate adherence and motility to maintain organized coherent motion<sup>1</sup>; extensive work continues to probe how cells establish such communication and organization<sup>2,3</sup>. Cells migrate collectively to build and vascularize tissues, heal wounds, and occasionally in tumor metastases. A comprehensive review of collective cell motility

\*Correspondence: zaman@bu.edu.

establishes the many modes of migration available to cell collectives as well as the forces that drive motility<sup>4</sup>. A broad classification for 3D collective migration modes can comprise of two categories— in the first, cells never dissociate from their original tissue, as in the case of branching morphogenesis, angiogenesis, and multicellular strand invasion of cancers; and in the second, a detached cluster moves through ECM and other non-motile cells as observed in cancer metastases and *Drosophila* border cells<sup>5,6</sup>.

From a mechanical and physical standpoint, time-lapse imaging and immunohistochemistry reveal relevant characteristics of collective cell migration (CCM)<sup>1,7,8</sup>. For example, in *Drosophila*, E-cadherin is essential for collective direction sensing<sup>9</sup>, and tissue rotation is essential for building an extracellular-matrix (ECM) to control egg shape<sup>10</sup>. In a 3D example, human mammary cells embedded in 3D gels reveal that rotation is essential to the formation of breast acini- it does not occur for cancerous breast cells, and when disrupted within normal cells, acini do not form<sup>11</sup>. Tracking assays on monolayers reveal density-dependent phase transitions<sup>12</sup>, substrate dependence<sup>13</sup>, and the forces driving CCM<sup>14,15</sup>. A comprehensive study of the mechanical properties of epithelial monolayers identified E-cadherin and P-cadherin as key proteins contributing to intercellular forces<sup>16</sup>. Heterogeneity emerges within groups of cells exhibiting collective behavior- functionally distinct populations of cells are termed leader and follower cells<sup>4</sup>. Leader cells are located at the front of a moving collective; they are responsible for receiving cues and directing the collective. Well-defined leader cells are found in cases of sprouting morphogenesis and angiogenesis<sup>17</sup>. In sheet migration, key molecules are upregulated to form leader cells at the leading edge; removal of these leader cells disrupts migration<sup>18</sup>.

Cancer pathologies are not amenable to direct observations of coherent translation due to diagnostic limitations; however, indirect evidence from *in vivo* measurements demonstrates that cancer metastases can migrate through tissue layers as collective masses<sup>5,6,19</sup>. Clinically, patients with epithelial-originating cancers or carcinomas present with circulating tumor microemboli, or clusters of circulating tumor cells up to 8 cells large<sup>20,21</sup>. Typical 3D studies of cell collectives involve immunohistochemistry assays and invasion assays of immortalized cancerous and non-cancerous cell lines. Immunohistochemistry has elucidated biochemical markers crucial to the emergence of leader-follower heterogeneity<sup>22</sup> in cancer cell lines. Invasion assays involve seeding a large spheroid (>200  $\mu\text{m}$  in diameter) of cancerous or non-cancerous cells into a 3D matrix; the subsequent invasion of the spheroid into the matrix can take the form of single cell invasion or multicellular strand invasion. Time-lapse microscopy conducted on invasion assays highlights cell dynamics, leader-cell formation<sup>23</sup>, and cell jamming<sup>24</sup>; together these data suggest that cancer cells have inherent plasticity of migration modes and the ability to transition between these modes<sup>25</sup>.

The dynamics of collective cell motility are essential to understanding collective processes and function. In 2D environments, epithelial cells and fish keratocytes<sup>26</sup> have been used as model systems to study the dynamic aspects of collective cell migration. Here, we present a model system for quantifying 3D collective migration using mammalian cell cohorts comprised of three to thirty-one cells. This can serve as a tool for understanding the motility of detached cellular clusters that have been observed in cancer metastases *in vitro* and found as circulating tumor microemboli *in vivo*. We track individual cells within cohorts embedded

in a 3D scaffold and identify events of emergent collective behavior in the absence of external driving agents. Our system serves as a 3D experimental model for collective motility of cells that is able to analyze each cell cohort as an individual entity. It is a first step toward a physical understanding of collective cell motility in 3D, including cancer cell invasion and the critical conditions that lead toward collective metastasis.

## Materials and Methods

### Cell Culture

MDCK Type II epithelial cells are propagated in monolayers at 37°C, 5% CO<sub>2</sub>, and ~ 70% humidity; monolayers are cultured in DMEM media supplemented with 10% fetal bovine serum and 1% penicillin/streptomycin. Cells are stably transfected to express Nuclear Localization Signal (NLS) bound to Green Fluorescent Protein (GFP). Transfection is accomplished by a GFP-NLS plasmid (Clontech, Takara Bio, Japan) of Lipofectamine 2000 (Invitrogen, Life Technologies, Grand Island, NY). To maintain fluorescence 0.5 mg/ml G418 is added to the media; Fluorescence Activated Cell Sorting (FACS) selects for the brightest 1% of cells. Identical procedures are followed on MDCK GFP-Ecad cell lines<sup>27</sup>.

### 3D Cluster protocol

Single cell suspensions are formed by immersing cells in media after trypsinization; cells are passed through a 40 µm cell strainer (BD Biosciences, San Jose, CA); cells are then seeded onto a 10 cm diameter Ultra Low Attachment Dish (Corning, Corning NY) with 10 ml media. After 48 hours, clusters are extracted by passing the solution through a 100 µm cell strainer followed by a 40 µm cell strainer, retaining clusters of 10–20 cells. These are resuspended and centrifuged at 800 rcf, and then immersed in a collagen solution for 3D culture and imaging.

A 2 mg/ml collagen dilution is obtained by mixing equal volumes of collagen Type 1 stock (BD Biosciences, San Jose, CA) solution and neutralizing buffer (100mM Hepes in 2x PBS, pH 7.3) with PBS. Cell clusters are added to the 2 mg/ml collagen solution; this cluster-collagen suspension is seeded onto several wells of a 24-well plate or 96 well-plate (MatTek, Ashland MA). The plates are incubated at 37°C, 5% CO<sub>2</sub> and ~ 70% humidity for 2 hours until the collagen has polymerized, after which ~1–2 ml of growth media is added to each well. FluoSpheres® Carboxylate-Modified Microspheres in 1.0 µm (Invitrogen) with red fluorescence (580/605) are diluted to ~ 10<sup>8</sup> beads/ml collagen when used.

### Imaging and Tracking

Images are acquired with a DMI600B Microscope (Leica, Solms, Germany) and ImagEM EM-CCD Camera (Hamamatsu Photonics, Hamamatsu, Japan) using a Spinning Disk Confocal setup (Yokogawa, Tokyo, Japan). Micro-Manager 1.4 Software (<http://www.micro-manager.org>) employs a 10× 0.3 NA objective lens to image ~560 × 560 × 100 µm<sup>3</sup> fields of view. 3D stacks are acquired in the XY plane with a Z-step of 4 µm, every 10 minutes, for ~48 hours over a 100–200 µm depth. For the experiment with GFP-Ecad a 20× 0.4 NA objective lens was used with a Z-step of 2 µm over a 42 µm depth. Cells can sense the substrate beneath the 3D matrix from inside the collagen gel<sup>28</sup>, and cells that are closer to

the glass bottom show very high proliferation along with sheet-like dynamics. Since the scope of this work pertains to 3D cell morphology, acquisition and analysis is restricted to cells clusters located  $>100\ \mu\text{m}$  from the glass bottom. 3D morphology is further verified before tracking and analysis.

ImageJ (NIH) is used to estimate the average nuclear diameter ( $\sim 8\ \mu\text{m}$ ). This diameter is input into a Matlab (MathWorks, Natick, MA) spot-tracking algorithm designed by the Kilfoil group<sup>29</sup>; the algorithm is modified for 3D nucleus detection and tracking. Parameters such as nucleus diameter, mask, minimum track time, and maximum displacement between consecutive time points, are optimized until varying each parameter independently has a minimal effect on the output. This metric is optimized until on average, 93% of all nuclei identified are assigned to a track. New cell identifiers are assigned when tracking is lost after 3 consecutive time points or after cell division. For a single track, if a cell is missing for up to two time points, its position is interpolated by assuming a straight path. A de-drifting algorithm designed by the Kilfoil group<sup>30</sup> eliminates net motion that is common to all cells in the 3-dimensional field of view to account for stage drift, which is  $\sim 25\text{--}40\ \mu\text{m}$  every 24 hours.

### Clustering Algorithm

A custom hierarchical clustering algorithm is written in Matlab to sort cells into cohorts, or groups of cells that are physically attached to each other. The algorithm is agglomerative—each cell is initially assigned a unique cluster identifier. For the first cell considered, all cells positioned within  $35\ \mu\text{m}$  are assigned to its cluster; all cells positioned within  $35\ \mu\text{m}$  of those cells are then assigned the same cluster. The process repeats until there are no cells that could be grouped into the same cluster; then the next cell with a unique cluster ID is considered. For these cells, a cutoff distance of  $35\ \mu\text{m}$  is empirically determined to be  $\sim 1.5$  3D cell lengths; thus minimizing the likelihood of skipping an adherent neighbor. Cutoff distances ranging between  $25\text{--}45\ \mu\text{m}$  do not affect the output data. A custom function auto-correlates cluster IDs between consecutive time-points to ensure that each cluster has a unique ID for the duration of the experiment. A cluster is reassigned the same ID if it retains a majority of cell IDs from the previous time point, such that if two cohorts merge, the new cluster is labeled as the larger of the two.

### Displacement Squared Quartiles and Order

Displacements of each cell in a cohort between time  $t + 0.5 * T_{int}$  and  $t - (0.5 * T_{int} + T)$  are calculated across the entire timespan of the experiment, where  $T_{int} = 1\ \text{h}$  and  $T = 10\ \text{min}$  (gap between consecutive time points). This results in a distribution with as many values as number of cells in the cohort at each time point. Displacements are squared, and the median, upper-quartiles, and lower-quartiles of this distribution are evaluated for all time points of the experiment. To calculate order parameter<sup>31</sup>, a smoothing function is run on XYZ position data between consecutive time points according to Equation 1 where  $x$  represents position and  $t$  represents time; the interval between consecutive data points is 10 minutes.

$$\vec{x}_t = \frac{\vec{x}_{t-\Delta T} + \vec{x}_t + \vec{x}_{t+\Delta T}}{3} \quad (1)$$

The  $T_{int}$  order parameter is calculated for the cohort between time  $t+0.5*T_{int}$  and  $t-(0.5*T_{int} + T)$  as shown in Equation 2 where  $v$  is velocity and  $N$  is the number of cells in the cohort.

$$\varphi(t) = \frac{\left| \sum_{i=1}^N \vec{v}_i T_{int} \right|}{\sum_{i=1}^N \left| \vec{v}_i T_{int} \right|} \quad (2)$$

$T_{int}$  is selected by studying Mean Squared Displacement (MSD) vs. time interval plots (data not shown) for all cells in the experiment. MSD plots suggest that the cells in these experiments have high heterogeneity of behavior over intervals as low as 30 minutes. In order to account for bias induced by tracking, de-drifting, and noise, we doubled this number to set  $T_{int} = 1$  h.

### Automated Event Selection

To analyze individual cohorts, a custom algorithm is written in Matlab to detect motility events from median displacement squared data. Initially, Matlab's built-in peak finding algorithm is used to find all peaks in the data. Peaks are merged if the valley between them  $> 0.5*P_{min}$  and the time gap between them  $< 1.5*T_{int}$ . Then peaks with width  $< T_{int}$  or height  $> P_{min}$  are eliminated.  $P_{min}$ , or the minimum peak height for a motility event, is conservatively set at  $60 \mu m^2$ , in order to track motion of  $\sim 1$  3D nucleus diameter and minimize the loss of relevant information.

### Pairwise Correlations

Once an event is identified, smoothed positions of cells for that event inform correlation functions between all possible cell pairs within a cohort. This correlation function is represented by Equation 3 where  $i$  and  $j$  are the cell pair,  $\tau$  is time difference,  $t$  is time, and  $v$  is the velocity<sup>32</sup>.

$$C_{i,j}(\tau) = \left\langle \left( \frac{\vec{v}_i}{|\vec{v}_i|} \right)_t \cdot \left( \frac{\vec{v}_j}{|\vec{v}_j|} \right)_{t+\tau} \right\rangle \quad (3)$$

This correlation function reaches a maximum peak value at a lag time  $\tau_c$ ; when a peak has a height  $> 0.5$ , a correlation is considered significant and  $\tau_c$  is retained. For positive  $\tau_c$ , cell  $i$  lags cell  $j$  with duration  $\tau_c$ ; conversely, for negative  $\tau_c$ , cell  $j$  lags cell  $i$  with duration  $\tau_c$ .

## Results

To investigate long term behavior and heterogeneity of motion in time, 3D cell tracking is performed on representative cell cohorts comprising 3–31 cells every 10 minutes over a duration of 48 hours. Positions, cell IDs, and cluster IDs for twelve cell cohorts are obtained from two different 2mg/ml collagen gels and five independent fields of view. Cohorts are

dynamic and exhibit spatial and temporal heterogeneity; behavior may include seemingly random movement, collective rotation, or collective translation. Planar projections and renderings of nuclear tracking at 0 h, 24 h and 48 h are represented in red, green and blue, respectively, in Figure 1. Two of the cohorts merge between 24 and 48 h, as visible in Figure 1 C and D. For this merging event, one cohort changes direction of motion in the second half of the experiment. Data for the other 3 fields of view is represented in Supplementary Figure 1; planar projection time-lapse videos and renderings of nuclear tracking are presented in Supplementary Videos 1–5. The videos qualitatively demonstrate rotation and translation of individual cohorts at various time-points; individual cohorts within a field of view may or may not be correlated to each other. To verify that motion is not caused by external ECM deformation, an experiment is performed using 1  $\mu\text{m}$  fluorescent beads embedded alongside the cells in the collagen matrix (Supplementary Video 6). This video suggested that the matrix is relatively stable except for perturbations caused in the vicinity of cohorts, likely due to pulling of the gel. GFP-Ecad planar projections are in Supplementary Video 7, illustrating that E-cadherin is membrane bound in the cohorts.

The heterogeneity of cohorts in time is determined by studying the individual cell displacements for each cohort. For the 48 hour experiment, 1-hour displacements for all cells in a cohort are calculated; these displacements are squared ( $|d^2|$ ), and the median of the resulting distribution is plotted corresponding to the left y-axis of Figure 2. The upper and lower quartiles for the same distributions are plotted in the gray regions around the lines representing the median. The motility events isolated are depicted in shaded vertical strips in Figure 2. Upon isolating motility events for each individual cohort, we find evidence of coherent rotation and translation within intervals ranging from 1 to 6 hours. For these 12 cohorts, a total of 61 motility events are obtained; five cohorts have 1–3 events, whereas those depicted in Figure 2 are motile for almost the entire duration of the experiment. Displacements and events for ten other cohorts are displayed in Supplementary Figure 2.

Order parameters provide a quantitative metric to measure the collectivity of systems. Establishing an order parameter for this system identifies the presence of translation, and also distinguishes between rotation and translation. For cells translating collectively, the order parameter is  $\sim 1$ , and for cells rotating collectively this parameter is low, between 0 – 0.5. For a cohort rotating about an axis in the center of the cohort, the order parameter is 0. For cohorts rotating about an off-center or external axis the order parameter is higher. This is because when the axis of rotation is in the middle of the cohort there is an average velocity of 0 within the cohort.

For the 48 h experiment, 1-hour order parameters are plotted corresponding to the right y-axis in Figure 2. All motility events are identified via peaks in displacement; translation events are accompanied by peaks in the order parameter; rotation events are accompanied by fluctuations or valleys in the order parameter (Figures 2 and Table 1). While translation occurs over durations of 1 to 6 hours, rotation only occurs in bursts of 1 to 2 hours (Figure 2, Table 1 and Figure 3). For selected motility events, metrics such as total displacement of the cohort, average order, and average number of cells are depicted in Table 1; metrics for all 61 events are in Supplementary Tables.

The highest observed translation event has a duration of 6 hours and measures  $\sim 90 \mu\text{m}$ , corresponding to  $\sim 8$  3D cell diameters. To visualize a few motility events, cell trajectories derived from raw data with events from four different cohorts are mapped in Figure 3. Panels A and B show rotation, Panels C and D show translation. Spots are colored to indicate the initial and final time point of cell tracks within the event.

Directional correlation functions, defined in Equation 3, probe the inter-cellular dynamics within each cohort during a motility event. For the four representative events depicted in Figure 3, leading and lagging times are calculated using pairwise correlation functions; normalized occurrence frequencies of these times are displayed in Figure 4. For all cohorts in motility events, most cell pairs have 0 time lag between trajectories. For the two translating events in panels C and D, some cell-pairs have lags up to 200 minutes. For the shorter rotating events, the range of lag times is relatively smaller. There is no clear correlation between the magnitude of this time lag and the distance between cells.

## Discussion and Conclusion

Conventional cell tracking research assumes that the behavior of cells in 2D and 3D is homogenous in time; information from all time points is averaged to deduce the timescales for various cellular behavior<sup>33</sup>. This is typically achieved by fitting cell trajectories to a stochastic random walk model<sup>34</sup> to evaluate speed and persistence of cells in 2D or 3D; however the basic assumptions of a persistent random walk fail in a system of cell collectives. Simplified versions of this analysis have been used on cell collectives in 3D to evaluate diffusion coefficients and angular velocity of human mammary cells<sup>11</sup>, however these techniques are inapplicable to data presented here, since the first assumption to evaluating Mean Squared Displacement vs. time-lag is temporal homogeneity. As evident in Figure 2 and Supplementary Figure 2, for cell cohorts in this study, temporal heterogeneity is observable in patterns of motion. These systems are not correlated within a single field of view over the duration of observation— there are intervals in which clusters move away (Supplementary Video 1, 4–7 s) and intervals in which the same clusters move toward each other and merge (Supplementary Video 1, 33–40 s). Not all cohorts are alike; some exhibit higher translation, rotation, and fluctuation than others. For example, Gel I View i Cohort #3 has fourteen high motility events of both translation and rotation, while Gel II View ii Cohort #1 has only one motility event of translation (Figure 2, and Supplementary Tables). Cells in 3D are smaller than their 2D counterparts- our average cohort diameter is on the order of 2D single cell lengths<sup>35</sup>, but in 3D, it spans  $\sim 6$ –15 cells (Figure 1, and Supplementary Figure 1). Thus, displacements on the order of tens of microns, which would not be relevant for 2D studies, mark coherent collective motility in these 3D studies (Figure 1 and 2).

Cell collective studies of epithelial monolayers typically calculate the velocity correlation length<sup>13,36,37</sup> of monolayers. This correlation length is the length at which a radius-dependent velocity-correlation function equals zero on average for the monolayer. These analyses are effective at characterizing properties and differences between 2D cellular systems; however the underlying assumption is constant cellular density. Constant density is neither feasible nor interesting for 3D-collectives, since it does not pertain to any known 3D

collective motility modes and cannot account for the ECM. Therefore analysis techniques from the field of collective motion<sup>31</sup> are adapted here, specifically order parameters<sup>1</sup> and directional correlation functions, which have successfully been used to characterize heterogeneity in pigeon flocks<sup>32</sup>. Order parameters are easily adapted for this study—instead of calculating the order for the entire field of view, order parameters can be calculated on a cohort-by-cohort basis. The larger trajectory lags between cell-pairs that occur within a translating cohort as observed in our system may represent information transfer and polarity along the cohort. The order parameter of cohorts is seldom lower than 0.2, and the quartiles follow the same trends as the median (Figure 2); thus there is a tendency for cells to stay within cohorts instead of splitting apart and invading the matrix. These results imply that cell-cell junctions contribute largely to cohort integrity and function. Indeed, GFP E-cadherin MDCK cell cohort experiments displayed E-cadherin localized at cell boundaries in 3D (Supplementary Video 6).

Many modes of collective cell motility have been observed in the presence of an external driving agent<sup>4</sup>. The results presented here suggest that the system of cell-matrix interactions is complicated and diverse enough to drive collective motion. Emergent motility events arise in the absence of external or forced driving agents, and are stochastic, as in the case of the two clusters that merged (Figure 1C and D). There are examples of other similarly sized clusters that do not merge and in fact move in opposite directions (Supplementary Figure 1E and F). The transient nature of these events suggests that this system displays stochasticity and plasticity, both suspected to occur in cancer pathologies.<sup>38</sup> Our setup provides a model system that allows for characterization of inter-cohort and intra-cohort dynamics as well as identification and analysis of emergent motility events. The techniques presented here could be applied to cancer explants, which are known to show coordinated collective motion *in vitro*<sup>5,6</sup>. As opposed to visually searching for motility, our work presents quantitative algorithms to isolate, observe, and characterize it. Since the methods operate on a cohort-by-cohort basis, they can be applied to a large amount of data and automated to extract motility events and compare different cellular cohorts.

Considering the balance of adherence and motility required for collective motion, translation over a few cell lengths in the absence of an external agent provides a promising model for the study of emergent phenomena and collective dynamics. Our results suggest that in the absence of external driving agents, interactions between cohorts and a collagen matrix are sufficient to drive collective cell motility. We show, for the first time, that cells spontaneously rotate in short bursts and translate for several hours; our analyses lay the foundation for quantitatively identifying supracellular polarity. The short bursts of rotation and comparatively larger spans of translation suggest that an internal stimulus arises within the dynamic cell-matrix system that attempts to drive collective translation. This work presents a quantitative approach to 3D cell collectives that have dynamic spatiotemporal heterogeneity—each cellular cohort is unique, and the algorithm finds motility events on a cohort-by-cohort basis. We built our custom algorithm using empirical data; however, it can be used for other cell types and experimental set-ups in order to probe questions of 3D collective mechanics, function, and efficiency. Our approaches can be expanded to study a range of phenomena in 3D, including collective cancer migration, density-dependent phase transitions, cell jamming, and emergent systems.



## Supplementary Material

Refer to Web version on PubMed Central for supplementary material.

## Acknowledgments

MDCK GFP-Ecad cell lines were a gift from Dr. James Nelson at Stanford. This work was supported by the National Science Foundation (DMR-1206335 and DMR-1310266), the National Institute of Health (BRP 1R01 HL107561-01, P01HL120839), the Harvard Materials Research Science and Engineering Center (DMR-1420570), and Boston University's XTNC fellowship of the NIH under Award Number NIH R25 CA153955. The content is solely the responsibility of the authors and does not necessarily represent the official views of the National Institutes of Health.

## References

1. Mehes E, Vicsek T. Collective motion of cells: from experiments to models. 2014; 21 arXiv Prepr. arXiv1403.1127. 10.1039/C4IB00115J
2. Rørth P. Collective cell migration. *Annu Rev Cell Dev Biol.* 2009; 25:407–29. [PubMed: 19575657]
3. Ilina O, Friedl P. Mechanisms of collective cell migration at a glance. *J Cell Sci.* 2009; 122:3203–8. [PubMed: 19726629]
4. Haeger A, Wolf K, Zegers MM, Friedl P. Collective cell migration: guidance principles and hierarchies. *Trends Cell Biol.* 2015; 25:556–566. [PubMed: 26137890]
5. Friedl P, Gilmour D. Collective cell migration in morphogenesis, regeneration and cancer. *Nat Rev Mol Cell Biol.* 2009; 10:445–57. [PubMed: 19546857]
6. Friedl P, et al. Migration of coordinated cell clusters in mesenchymal and epithelial cancer explants in vitro. *Cancer Res.* 1995; 55:4557–60. [PubMed: 7553628]
7. Weijer CJ. Collective cell migration in development. *J Cell Sci.* 2009; 122:3215–23. [PubMed: 19726631]
8. Rørth P. Collective guidance of collective cell migration. *Trends Cell Biol.* 2007; 17:575–9. [PubMed: 17996447]
9. Cai D, et al. Mechanical feedback through E-cadherin promotes direction sensing during collective cell migration. *Cell.* 2014; 157:1146–59. [PubMed: 24855950]
10. Haigo SL, Bilder D. Global tissue revolutions in a morphogenetic movement controlling elongation. *Science.* 2011; 331:1071–1074. [PubMed: 21212324]
11. Tanner K, Mori H, Mroue R, Bruni-Cardoso a, Bissell MJ. Coherent angular motion in the establishment of multicellular architecture of glandular tissues. *Proc Natl Acad Sci.* 2012; 109:1973–1978. [PubMed: 22308439]
12. Szabó P, Nagy M, Vicsek T. Transitions in a self-propelled-particles model with coupling of accelerations. *Phys Rev E Stat Nonlin Soft Matter Phys.* 2009; 79:021908. [PubMed: 19391779]
13. Doxzen K, et al. Guidance of collective cell migration by substrate geometry. *Integr Biol (Camb).* 2013; 5:1026–35. [PubMed: 23784144]
14. Brugués A, et al. Forces driving epithelial wound healing. *Nat Phys.* 2014; 10:683–690.
15. Shaw TJ, Martin P. Wound repair at a glance. *J Cell Sci.* 2009; 122:3209–13. [PubMed: 19726630]
16. Bazellères E, et al. Control of cell-cell forces and collective cell dynamics by the intercellular adhesome. *Nat Cell Biol.* 2015; 17:409–420. [PubMed: 25812522]
17. Riahi R, et al. Notch1-Dll4 signalling and mechanical force regulate leader cell formation during collective cell migration. *Nat Commun.* 2015; 6:6556. [PubMed: 25766473]
18. Yamaguchi N, Mizutani T, Kawabata K, Haga H. Leader cells regulate collective cell migration via Rac activation in the downstream signaling of integrin  $\beta$ 1 and PI3K. *Sci Rep.* 2015; 5:7656. [PubMed: 25563751]
19. Deisboeck TS, Couzin ID. Collective behavior in cancer cell populations. *Bioessays.* 2009; 31:190–7. [PubMed: 19204991]

20. Hou J-M, et al. Circulating tumor cells as a window on metastasis biology in lung cancer. *Am J Pathol.* 2011; 178:989–96. [PubMed: 21356352]
21. Carlsson A, et al. Circulating Tumor Microemboli Diagnostics for Patients with Non–Small-Cell Lung Cancer. *J Thorac Oncol.* 2014; 9:1111–1119. [PubMed: 25157764]
22. Khalil, Aa; Friedl, P. Determinants of leader cells in collective cell migration. *Integr Biol (Camb).* 2010; 2:568–74. [PubMed: 20886167]
23. Carey SP, Starchenko A, McGregor AL, Reinhart-King CA. Leading malignant cells initiate collective epithelial cell invasion in a three-dimensional heterotypic tumor spheroid model. *Clin Exp Metastasis.* 201310.1007/s10585-013-9565-x
24. Haeger A, Krause M, Wolf K, Friedl P. Cell jamming: collective invasion of mesenchymal tumor cells imposed by tissue confinement. *Biochim Biophys Acta.* 201410.1016/j.bbagen.2014.03.020
25. Friedl P, Alexander S. Cancer invasion and the microenvironment: plasticity and reciprocity. *Cell.* 2011; 147:992–1009. [PubMed: 22118458]
26. Rapanan JL, Cooper KE, Leyva KJ, Hull EE. Collective cell migration of primary zebrafish keratocytes. *Exp Cell Res.* 2014; 326:155–65. [PubMed: 24973510]
27. Adams CL. Mechanisms of Epithelial Cell-Cell Adhesion and Cell Compaction Revealed by High-resolution Tracking of E-Cadherin-Green Fluorescent Protein. *J Cell Biol.* 1998; 142:1105–1119. [PubMed: 9722621]
28. Leong WS, et al. Thickness sensing of hMSCs on collagen gel directs stem cell fate. *Biochem Biophys Res Commun.* 2010; 401:287–92. [PubMed: 20851103]
29. Gao Y, Kilfoil ML. Accurate detection and complete tracking of large populations of features in three dimensions. *Opt Express.* 2009; 17:4685–704. [PubMed: 19293898]
30. Pelletier V, Gal N, Fournier P, Kilfoil ML. Microrheology of Microtubule Solutions and Actin-Microtubule Composite Networks. *Phys Rev Lett.* 2009; 102:188303. [PubMed: 19518917]
31. Vicsek T, Zafeiris A. Collective motion. *Phys Rep.* 2012; 517:71–140.
32. Nagy M, Akos Z, Biro D, Vicsek T. Hierarchical group dynamics in pigeon flocks. *Nature.* 2010; 464:890–3. [PubMed: 20376149]
33. Zaman MH, et al. Migration of tumor cells in 3D matrices is governed by matrix stiffness along with cell-matrix adhesion and proteolysis. *Proc Natl Acad Sci U S A.* 2006; 103:10889–94. [PubMed: 16832052]
34. Dickinson RB, Tranquillo RT. Optimal estimation of cell movement indices from the statistical analysis of cell tracking data. *AIChE J.* 1993; 39:1995–2010.
35. Sepúlveda N, et al. Collective Cell Motion in an Epithelial Sheet Can Be Quantitatively Described by a Stochastic Interacting Particle Model. *PLoS Comput Biol.* 2013; 9:e1002944. [PubMed: 23505356]
36. Tambe DT, et al. Collective cell guidance by cooperative intercellular forces. *Nat Mater.* 2011; 10:469–475. [PubMed: 21602808]
37. Das T, et al. A molecular mechanotransduction pathway regulates collective migration of epithelial cells. *Nat Cell Biol.* 2015; 17:276–287. [PubMed: 25706233]
38. Friedl P, Hegerfeldt Y, Tusch M. Collective cell migration in morphogenesis and cancer. *Int J Dev Biol.* 2004; 48:441–9. [PubMed: 15349818]

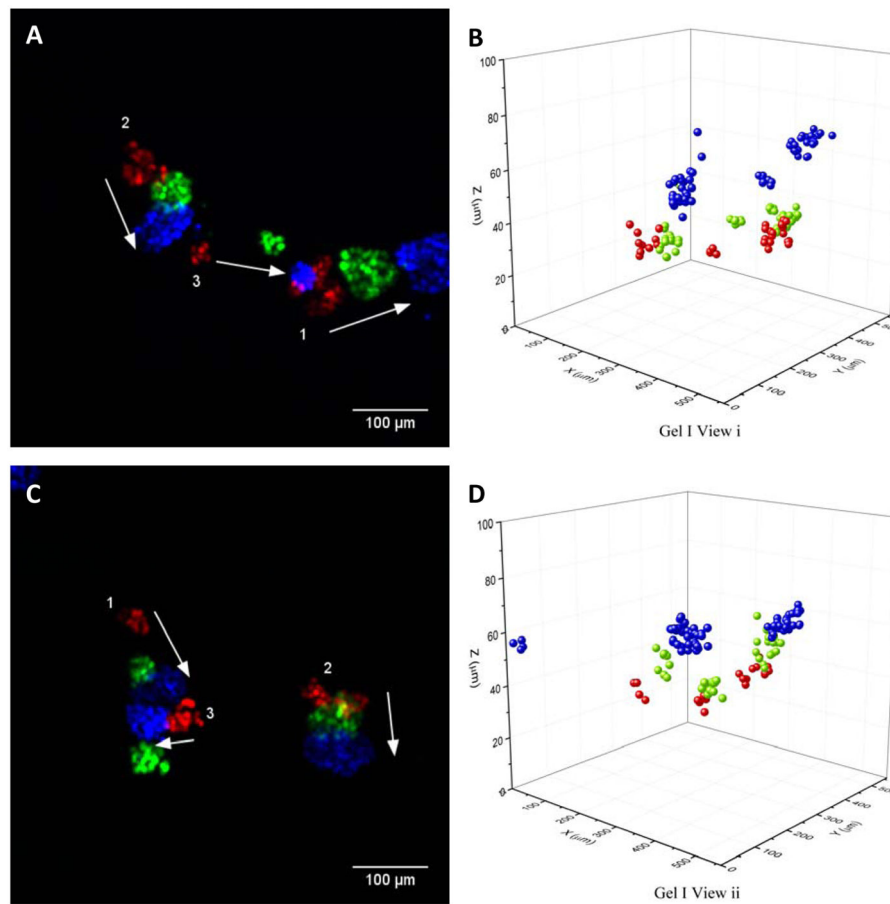


**Figure 1.** Panels A and C show Z-projections of 2 fields of view from the same 3D collagen gel with MDCK GFP-NLS cell cohorts at 0 h (red), 24 h (green) and 48 h (blue). The numbers in white indicate cohort number as determined by a clustering algorithm. Panels B and D are 3D renderings of nuclear tracking corresponding to Panel A and C respectively.

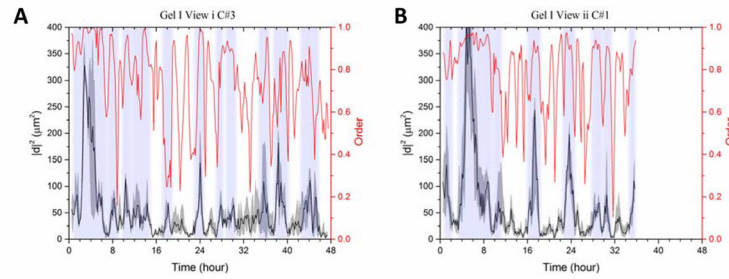


**Figure 2.**

Panel A has temporal analysis for Gel I View i Cohort #3, and Panel B has the same for Gel I View ii Cohort #1. The left y-axis corresponds to the 1h squared displacement distribution: black line is the median, grey shaded regions are upper and lower quartiles. Vertical shaded regions represent motility events. The right y-axis and the red line correspond to 1h order parameter of the cohort.

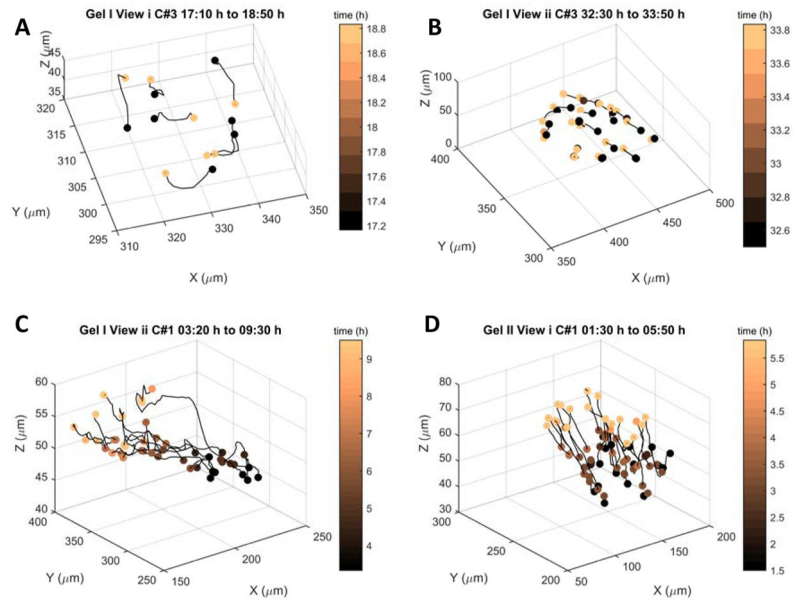


**Figure 3.** Cell trajectories extracted from raw data for four different events and cohorts. Each cell track is represented by a single black line. Colors of spots mark initial and final time for each track. Panels A and B depict rotation, panels C and D depict translation.

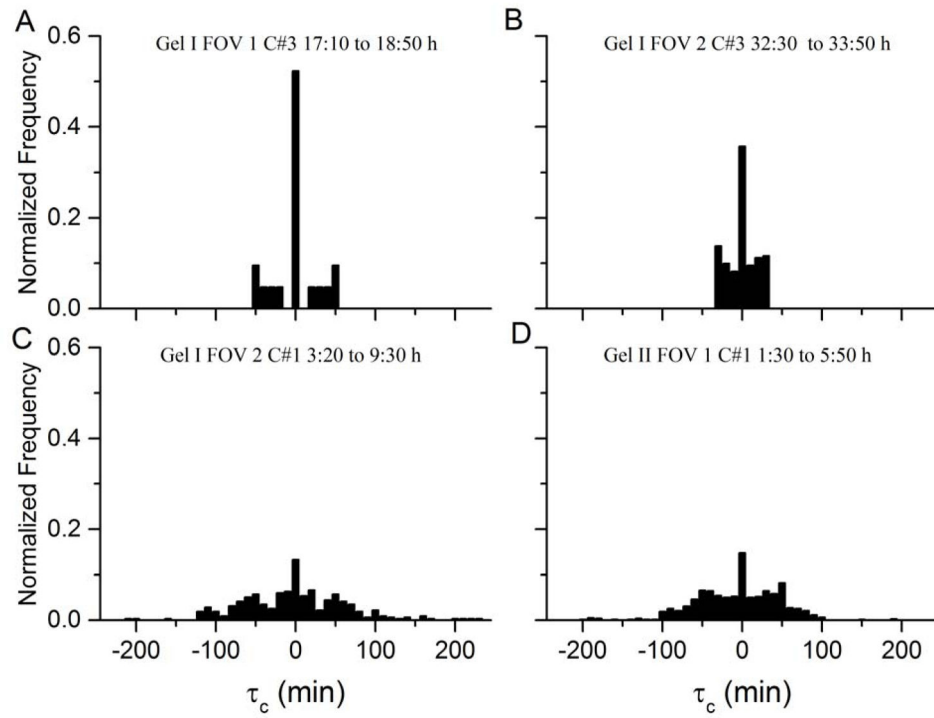


**Figure 4.**

For four events, these histograms show the normalized occurrence frequency of leading and lagging times  $\tau_c$ .  $\tau_c$  is obtained from pair-wise correlation functions, and it represents the time lag at which the function has a peak above 0.5, indicating the delay between cell trajectories.

Parameters of four motility events. C is Cohort ID, T<sub>i</sub> is the initial time, T<sub>f</sub> is the final time, |d| is the displacement of the cohort,  $\langle\phi\rangle$  is the average order, and N<sub>c</sub> is the average number of cells in the cohort

**Table 1**

Gel	View	C	T <sub>i</sub> (h)	T <sub>f</sub> (h)	d  (μm)	$\langle\phi\rangle$	N <sub>c</sub>
I	i	3	17:10	18:50	3.35	0.39	7
I	ii	1	3:20	9:30	89.06	0.92	10
II	i	1	1:30	5:50	53.09	0.84	19
I	ii	3	32:30	33:50	6.33	0.72	23